

Supporting Information

Ultrathin TiO₂-coated MWCNTs with Excellent Conductivity and SMSI nature as Pt Catalyst Support for Oxygen Reduction Reaction in PEMFCs

Nibret Gebeyehu Akalework,^a Chun-Jern Pan,^a Wei-Nien Su,^a John Rick,^a Mon-Che Tsai,^a Jyh-Fu Lee,^b, Jhih-Min Lin^b, Li Duan Tsai,^c and Bing-Joe Hwang,^{*,a,b}

^aNanoElectrochemistry Laboratory, Department of Chemical Engineering,
National Taiwan University of Science and Technology, Taipei, 106, Taiwan

^bNational Synchrotron Radiation Research Center, Hsinchu, 30076, Taiwan

^cDepartment of Fuel Cell Materials and Advanced Capacitors, Division of Energy Storage
Materials and Technology, Material and Chemical Laboratories, Industrial Technology Research
Institute, HsinChu, 300, Taiwan

*Corresponding Author. Fax: +886-2-27376644, E-mail: bjh@mail.ntust.edu.tw

^aCurrent address: National Taiwan University of Science and Technology, Taipei 106, Taiwan

The following supporting information is included:

1. List of materials and chemicals used for synthesis of Pt/MWCNT@UT-TiO₂
2. Characterization
3. Raman (a), FT-IR spectra (b) and TGA spectral (c) patterns of pristine MWCNT and acid treated MWCNT (Figure S1).
4. Elemental mapping images of Pt/MWCNT@UT- TiO₂ electrocatalyst (Figure S2)
5. Computational detail
6. General view of anatase-TiO₂ (101) surface (Figure. S3)
7. Deconvoluted C1s peaks from High-resolution XPS analysis of MWCNT, MWCNT@UT- TiO₂, Pt/MWCNT@UT- TiO₂ and Pt/MWCNT (Figure S4)
8. Ti2p and Deconvoluted O1s peaks from XPS analysis of MWCNT@UT-TiO₂, Pt/MWCNT@Ut-TiO₂, Pt/MWCNT, acid treated MWCNT, Pt4f (Figure S5).
9. Results of the fits of the O1s spectra, values given in binding energy and % of the total intensity (Table S1)
10. Pt4f peaks from XPS analysis of Pt/MWCNT@TiO₂ and Pt/MWCNT (a) and Ti2p peaks from Pt/MWCNT@UT-TiO₂ and MWCNT@UT-TiO₂ (b) (Figure. S6).
11. Details on number of unfilled d states (h_{Ts}) Calculation

Materials

Pristine multiwalled CNTs (OD 10-20 nm, L 5-15 μm , average specific surface area, 160 m^2/g , purity >95%) was purchased from Scientech Corporation. Tetrabutyltitanate (Ti(OBu)_4 , 99%,), Hydrogen hexachloroplatinate (IV) hexahydrate ($\text{H}_2\text{Cl}_6\text{Pt.6H}_2\text{O}$, 99.9%), 1-Propanol (99% extra pure) and Ethylene Glycol ($\text{C}_2\text{H}_6\text{O}_2$, 99 %) were from Acros Organics, sulfuric acid (H_2SO_4 , 98 %) from ScharlauChemi S.A, and nitric acid (HNO_3 , 65 %) was obtained from Panreac. SERVAPOR(R) dialysis tubing (diameter 50 mm MWCO 12,000-14,000) and Nafion 117 solution were from Aldrich.

Characterization

Raman spectra were collected using a RamanRxn1 equipped with a holographic notch filter at 785 nm, and a DPSS Laser (Red Laser) light source, to excite the samples. FTIR spectra were recorded using a Digital FT3500 spectrometer. Thermogravimetric analysis (TGA) of the synthesized materials was performed with a Diamond TG/ DTA instrument (Perkin Elmer) under air with a scan rate of 20 $^{\circ}\text{Cmin}^{-1}$.

Raman spectroscopy was used to study the surface structure of pristine MWCNTs and acid treated MWCNTs, as shown in **Figure. S1a**. Both of these MWCNTs have similar Raman scattering patterns. The peaks near 1313 cm^{-1} and 1596 cm^{-1} are assigned to the disordered diamond structure (D-band, sp^3 hybridized carbon) and to a splitting of the E_{2g} stretching mode of graphite (G-band, sp^2 hybridized carbon), which reflects the structural intensity of the sp^3 and sp^2 -hybridized carbon atoms respectively.¹ It is observed that G band splitting of MWCNT is both small in intensity and smeared out due to the effect of the diameter distribution within the individual MWCNT, and because of the variation between different tubes in an ensemble of MWCNT in typical experimental samples. Therefore, the G-band feature predominantly exhibits a weakly asymmetric characteristic line shape, with a peak appearing close to the graphite frequency. Thus the extent of modified carbon or defects in MWCNTs can be evaluated by the intensity ratio of the D- and G-bands: the $I_{\text{D}}/I_{\text{G}}$ ratio is 1.21 for pristine MWCNTs and 1.60 acid treated MWCNTs respectively. In the case of acid treated carbon material, the intensity of the D-band increases compared to that in the pristine MWCNT. During acid treatment, carbon

associated with carboxylic, epoxy or hydroxyl groups is transformed from a planar sp^2 -hybridized state to a distorted sp^3 -hybridized geometry.²⁻⁴

Fig.S1b shows IR spectra in the region 4000–400 cm^{-1} for pristine MWCNT and acid treated MWCNT. Pristine MWCNTs have characteristic bands at: 1560 cm^{-1} corresponding to the graphitic structure of the sp^2 -hybridized carbon in MWCNTs, 1637 cm^{-1} (attributed to -OH bend) and 1025 cm^{-1} (corresponding to C-O stretching mode in alcohols). The peak at 3426 cm^{-1} is assigned to -OH stretching, while those at ~2920 and ~2850 cm^{-1} are due to asymmetric and symmetric CH stretching modes. Bands at 1384, 1739 and 1457 cm^{-1} are also apparent -the former is attributed to a CH bending mode, while the latter two originate from carboxylic C=O vibrations. These results show that the pristine MWCNT's surface contains some oxygen containing groups. The acid treated MWCNT IR spectra shares similar basic features with that of the pristine MWCNT. However the peak intensity increase at 3426 cm^{-1} together with the peak shift at 1784 cm^{-1} indicates an increased number of carboxylic acid groups on the surface of the MWCNTs, thereby showing that the acid treatment facilitated the grafting of oxygen-bearing groups on the surface of the MWCNTs.^{5,6} In order to measure the relative purity of the pristine and treated MWCNTs, thermogravimetric analysis was performed under air. **Fig.S1c** shows the TGA curves of pristine MWCNTs and acid treated MWCNTs from room temperature to 850 °C, at a heating rate of 10 °C/min. It shows that the main weight loss occurs between 500–630 °C, which corresponds to the decomposition of MWCNTs.⁷ Clearly the curves of the pristine MWCNT and the acid treated MWCNT show the residues to retain 7.2 % and 3.2 %, of their original weights respectively. The decreases in weight percent after treatment can be attributed to the metal catalyst used for the synthesis of MWCNT being removed by the acid treatment.⁸

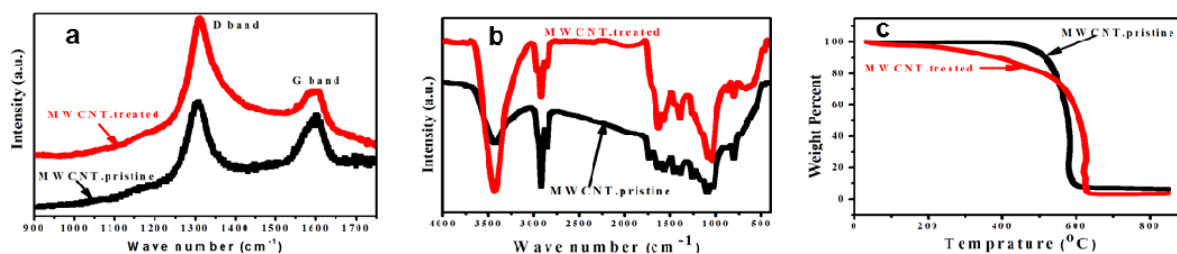


Figure S1 (a) Raman, FT-IR spectra (b) and TGA spectral (c) patterns of pristine MWCNT and acid treated MWCNT.

Fig.S2 presents TEM elemental mapping images of Pt/MWCNT@UT-TiO₂ electrocatalyst showing uniform distribution of Pt, C, O and Ti.

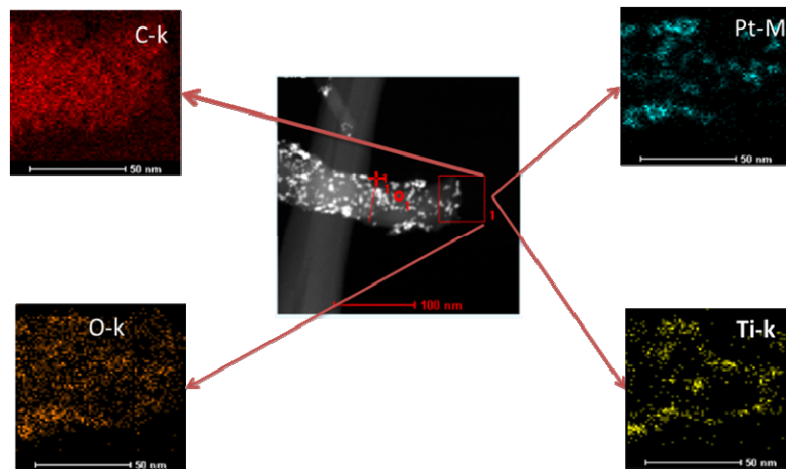


Figure S2 Elemental mapping images of Pt/MWCNT@UT-TiO₂ electrocatalyst

Computational detail

Density functional theory (DFT) calculations were performed to investigate the interaction of Pt and the TiO₂ substrate using plane-wave-pseudo potential within projector augmented wave method (PAW),⁹ together with the PW91-GGA exchange correlation functional as implemented in the VASP²¹⁰⁻¹² (Vienna Ab Initio Simulation Package). In the plane wave calculations, a cutoff energy of 400 eV was applied, which was automatically set by the total energy convergence calculation.

TiO₂ substrate was constructed as a slab model contains three TiO₂ (101) planes and models were separated from their images in the direction perpendicular to the surface by a 14 Å vacuum layer. The bottom one TiO₂ layer was kept fixed to the bulk coordinates; full atomic relaxations were allowed for the top two TiO₂ layers. In this calculation, a 3x3x1 *k*-Point mesh was used in the 2x 3 super cell.

In order to obtain the charge transfer between Pt and TiO₂ substrate, Bader charge analysis was carried out using DFT calculations. To evidence the experimental results, we introduced an oxygen vacancy to the anatase-TiO₂ (101) as the computational model, as shown in **Fig. S3**. In HAADF-STEM images of Pt/MWCNT@UT-TiO₂ (**Fig. 4b**), inset shows that single Pt atom adsorbs on the oxygen vacancy (Ti-Ti bridge site) of TiO₂ (101) surface, which indicates that electron transfer is induced from TiO₂ substrate to Pt atom, which is consistent with our XAS result.

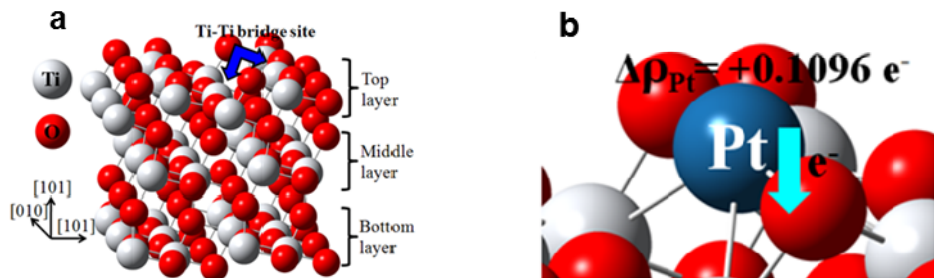


Figure S3 (a) general view of anatase-TiO₂ (101) surface and (b) electron transfer from Pt to support on non-reduced surface. Blue arrow (Fig S3 a) indicates oxygen vacancy (Ti-Ti bridge site) and the arrow (Fig 3b) shows electron transfer.

Fig. S4 shows deconvoluted C1s peaks from high-resolution XPS analysis of MWCNT, Pt/MWCNT, MWCNT@UT-TiO₂ and Pt/MWCNT@UT-TiO₂.

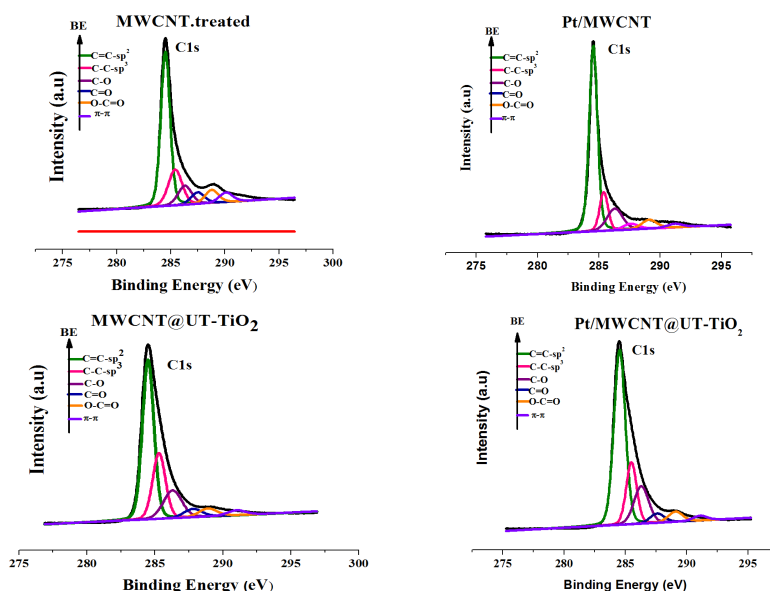


Figure S4 Deconvoluted C1s peaks from High-resolution XPS analysis of MWCNT, MWCNT@UT-TiO₂, Pt/MWCNT@UT-TiO₂ and Pt/MWCNT

Ti2p peaks from MWCNT@UT-TiO₂ and Pt/MWCNT@UT-TiO₂ XPS analysis and deconvoluted O1s peaks from XPS analysis of acid treated MWCNT, MWCNT@UT-TiO₂, Pt/MWCNT and Pt/MWCNT@UT-TiO₂ are shown in Fig. S5.

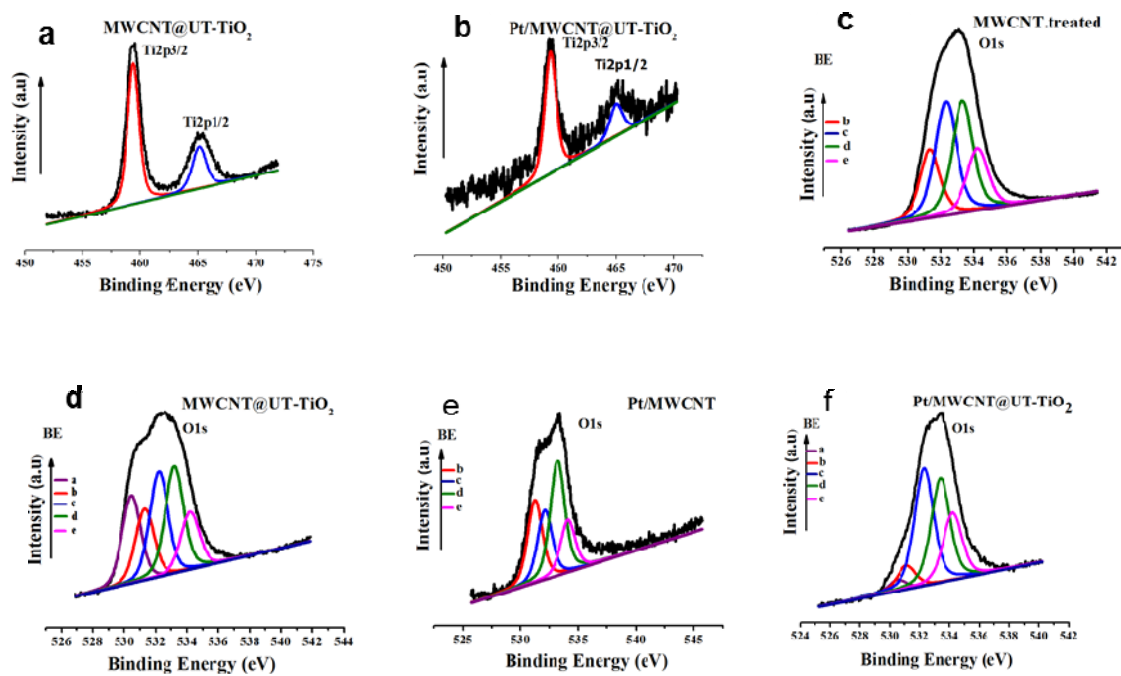


Figure S5 (a, b) Ti2p peaks from XPS analysis and (c,d,e,f) deconvoluted O1s of MWCNT@TiO₂ (a,d), Pt/MWCNT@TiO₂ (b, e), Pt/MWCNT (f) and acid treated MWCNT (c), (Legend a (at 530.5 eV) is Ti-O, b (at 531.2 eV) is C=O groups (carbonyl oxygen of esters, anhydrides); c(at 532.25 eV) is oxygen atoms in hydroxyls or ethers, d (at 533.3 eV) is ether oxygen atoms in esters and anhydrides, e (at 534.2 eV) is for oxygen atoms in carboxyl groups.

Following **table S1** presents the O1s binding energies of all components along with their relative intensities for acid treated MWCNT, MWCNT@UT-TiO₂, Pt/MWCNT@UT-TiO₂ and Pt/MWCNT.

Table S1 Results of the fits of the O1s spectra, values given in binding energy and % of the total intensity

Sample	530.5 eV	531.2 eV	532.25 eV	533.3 eV	534.2 eV
MWCNT.treated	-----	18.34	32.14	31.84	17.68
MWCNT@UT-TiO ₂	20.06	16.50	24.46	25.51	13.47
Pt/MWCNT@UT-TiO ₂	14.71	17.57	24.40	22.13	21.19
Pt/MWCNT	-----	25.62	21.64	36.26	16.48

Fig.S6 a shows lightly lower binding energy shift of Pt 4f of Pt/MWCNT@UT-TiO₂ compared with Pt/MWCNT and the commensurate higher binding energy shift of Ti2p of Pt/MWCNT@UT-TiO₂ compared with MWCNT@UT-TiO₂ (**Fig.S6 b**).

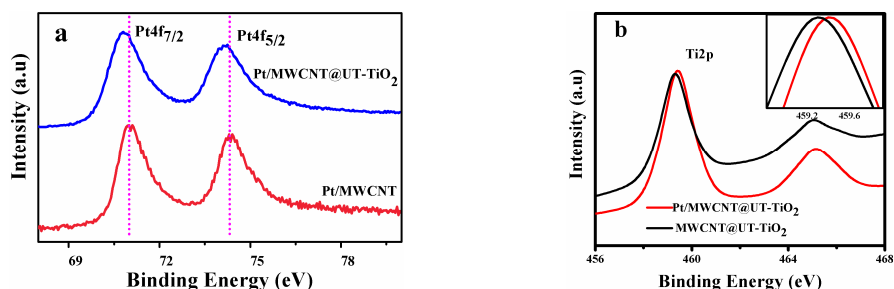


Figure S6 (a) XPS analysis of Pt 4f peaks from Pt/MWCNT@TiO₂ and (b) Pt/MWCNT and Ti 2p peaks from Pt/MWCNT@UT-TiO₂ and MWCNT@UT-TiO₂

Number of unfilled d states (h_{Ts}) Calculation

The number of unfilled d-states (h_{Ts}) of Pt/MWCNT@UT-TiO₂ and Pt/MWCNT were quantified and compared to the reference Pt foil (f_d) by a method developed elsewhere in the literature^{13, 14} using the equation.

$$f_d = \frac{\sigma_3 \Delta A_3 + (1.11 \sigma_2 \Delta A_2)}{\sigma_3 A_{3r} + (1.11 \sigma_2 A_{2r})} \quad (\text{S1})$$

Where ΔA_2 and ΔA_3 are the areas corresponding to electronic transitions to unfilled d-states in the XANES spectra between samples and the reference foil for L_{II}- and L_{III}-edges, respectively. ΔA_2 and ΔA_3 were calculated by subtracting the reference platinum foil data from the catalyst data and then numerically integrating the resulting curves between -10 and +14 eV for L_{II}- and L_{III}-edges. A_{2r} and A_{3r} are the areas corresponding to electronic transitions to unfilled d-states in the XANES spectra for the reference Pt foil for L_{II}- and L_{III}-edges, respectively. All the areas (A_{2r} , A_{3r} , ΔA_2 and ΔA_3) were normalized by multiplying with the X-ray absorption cross section (σ) at the respective edge jump. Values of 54.2 and 117.1 cm² g⁻¹ were used for the σ at the Pt L_{II}- and L_{III}-edges, respectively.¹⁴ Once the d-band vacancy in the reference material, h_{Tr} is known, the d-band vacancy of the sample h_{Ts} can be calculated by using equation

$$h_{Ts} = (1 + f_d)h_{Tr}, \quad (\text{S2})$$

where h_{Tr} is the number of unfilled d states in the Pt foil reference sample, which is a known quantity for 1.6.

Reference

1. C. Vix-Guterl, M. Couzi, J. Dentzer, M. Trinquecoste and P. Delhaes, *The Journal of Physical Chemistry B*, 2004, **108**, 19361-19367.
2. T. T. Baby and S. Ramaprabhu, *Nanoscale*, 2011, **3**, 2208.
3. F.-J. Lai, L. S. Sarma, H.-L. Chou, D.-G. Liu, C.-A. Hsieh, J.-F. Lee and B.-J. Hwang, *The Journal of Physical Chemistry C*, 2009, **113**, 12674-12681.
4. E. F. Antunes, A. O. Lobo, E. J. Corat, V. J. Trava-Airoldi, A. A. Martin and C. Veríssimo, *Carbon*, 2006, **44**, 2202-2211.
5. Q. R. Deng, X. H. Xia, M. L. Guo, Y. Gao and G. Shao, *Materials Letters*, 2011, **65**, 2051-2054.
6. V. T. T. Ho, C.-J. Pan, J. Rick, W.-N. Su and B.-J. Hwang, *Journal of the American Chemical Society*, 2011, **133**, 11716-11724.
7. D. Shao, Z. Jiang, X. Wang, J. Li and Y. Meng, *The Journal of Physical Chemistry B*, 2009, **113**, 860-864.
8. J.-M. Moon, K. H. An, Y. H. Lee, Y. S. Park, D. J. Bae and G.-S. Park, *The Journal of Physical Chemistry B*, 2001, **105**, 5677-5681.
9. G. Kresse and D. Joubert, *Physical Review B*, 1999, **59**, 1758-1775.
10. G. Kresse and J. Furthmüller, *Computational Materials Science*, 1996, **6**, 15-50.
11. G. Kresse and J. Furthmüller, *Physical Review B*, 1996, **54**, 11169-11186.
12. G. Kresse and J. Hafner, *Physical Review B*, 1993, **47**, 558-561.
13. S. N. Reifsnyder, M. M. Otten, D. E. Sayers and H. H. Lamb, *The Journal of Physical Chemistry B*, 1997, **101**, 4972-4977.
14. A. N. Mansour, J. W. Cook and D. E. Sayers, *The Journal of Physical Chemistry*, 1984, **88**, 2330-2334.